A Simple Model for Small Collections of Magnetic Plasmonic Oligomers

Nicholas P. Montoni, Steven C. Quillin, Charles Cherqui, and David J. Masiello*

Department of Chemistry, University of Washington, Seattle, WA 98195

E-mail: masiello@chem.washington.edu

Abstract

Ring-like assemblies of metal nanoparticles that exhibit magnetic resonances, called magnetic plasmon oligomers, have been of recent interest as negative-index metamaterials and light-harvesting devices. For these reasons, it is imperative to understand the properties of such systems on scales from single monomers to many. We show through theory and simulation that the energy ordering of the magnetic resonances of few-monomer oligomers depends greatly on the size, scale, and environment of the nanoparticle assembly in ways that purely electric plasmons do not. We show that the dynamic ordering of the eigenmodes of magnetic systems is due entirely to retardation effects and can be understood by inspecting closely the intermediate- and far-field contributions which are usually ignored in the quasistatic approximation. We show that magnetic systems are versatile and suggest experimental methods to directly determine magnetic mode energy-ordering. Finally, we make suggestions for future theoretical and experimental studies, as well as applications, of magnetic oligomer systems.

Abbreviations

MNP, LSPR, EELS

Keywords

plasmon, hybridization, magnetic, retardation

Introduction

Metal nanoparticles (MNPs) support collective resonances of thier conduction electrons at optical frequencies. These localized surface plasmon resonances (LSPRs) can interact with each other in assemblies of two or more MNPs to produce hybridized resonances of the assembly, much like the hybridization of atomic orbitals in molecules.[1–4] When these assemblies are arranged in rings, the single LSPRs can give rise to a collective mode that produces an oscillating magnetic dipole in he center of the ring.[5–10] Such systems are known as magnetic plasmon oligomers and have been of intense focus due to their potential applications in sensing,[11–18] lensing, cloaking, and information processing.[19–21] This work is motivated by the need to further explain previous results in the field.[9] In Cherqui's 2014 work on magnetic plasmons, a quasistatic, electric dipole tight-binding model was used to describe the magnetic systems. The model used later in this paper was built from this original model, and will be explained further. The original model considered only the electric near-field of the single-particle plasmons and only incorporated nearest-neighbor interactions. Comparison of this simple model with full-wave simulations led to a discrepancy: though the simple model accurately predicted the nature of the eigenmodes, it inaccurately described their energy-ordering, *i.e.* the spectrum of magnetic modes. An explanation was needed to determine why the tight-binding model would predict different energy-ordering than full-wave simulations.

In a recent paper, Engheta *et al.* state that magnetic systems are well-understood on the single oligomer scale and the nearly infinite scale.[22] However, the properties of collections of few magnetic oligomers have not been fully explored. Furthermore, the dependence of the magnetic properties of the systems on individual nanoparticle geometry and the relative size of the constituent oligomers has also been determined.[10] Here we show that to fully

understand the properties of magnetic oligomers on the few-oligomer scale, the simple tight-binding model described above must be extended to include both the fully-retarded electric fields and all inter-particle interactions. We show this through three explorations of oligomer properties: system size, embedding dielectric constant, and inter-particle spacing, and we confirm our results using full-wave simulations.[23]

It is well-known that as MNPs and MNP aggregates become larger, the quasistatic approximations breaks down. There has been much work done to elucidate the effects of retardation on large MNPs,[24,25] MNP dimers,[26–28] and extended 2-D arrays of particles.[29–31] Magnetic oligomers composed of two or more rings of particles have the potential to be hundreds of nanometers to microns across, justifying the need to consider retardation effects in determining their optical properties. In order to incorporate retardation effects into quasistatic plasmon hybridization theory, we begin by mapping the dipole plasmon of each MNP onto a set of harmonic oscillators, and allow them to couple through their electric fields according to the following Hamiltonian:

$$H = \sum_{i}^{n} \frac{\mathbf{P}_i^2}{2m_{\mathrm{sp},i}} + \frac{1}{2} m_{\mathrm{sp},i} \omega_{\mathrm{sp},i}^2 \mathbf{X}_i^2 - e^2 \sum_{i \neq j} \mathbf{X}_i \cdot \mathbf{\Lambda}_{ij} \cdot \mathbf{X}_j, \tag{1}$$

where $\mathbf{P}_i$ are the momenta conjugate to the coordinates $\mathbf{X}_i$, $\omega_{\mathrm{sp},i}$ are the individual LSPR frequencies of each oscillator, $m_{\mathrm{sp},i}$ are the LSPR effective masses and $\mathbf{\Lambda}_{ij}$ is the fully retarded dipole-dipole relay tensor (expanded below).[32] To make this Hamiltonian more manageable, it is nondimensionalized using $\mathbf{Q}_i = (m_{\mathrm{sp}}\omega_{\mathrm{sp}}/\hbar)^{\frac{1}{2}}\, \mathbf{X}_i$ and $\mathbf{\Pi}_i = \mathbf{P}_i / \sqrt{\hbar m_{\mathrm{sp}} \omega_{\mathrm{sp}}}$. Substituting into Equation 1 and expanding $\mathbf{\Lambda}_{ij}$, we get:

$$\begin{aligned} H = \frac{\hbar\omega_{sp}}{2} \sum_{i}^{n} [\mathbf{\Pi}_i^2 + \mathbf{Q}_i^2] - \frac{\hbar\omega_{sp}}{2\varepsilon_b} \sum_{i \neq j} \{ & g_{ij}^{\mathrm{NF}} \left[3(\mathbf{Q}_i \cdot \hat{\mathbf{n}}_{ij})(\hat{\mathbf{n}}_{ij} \cdot \mathbf{Q}_j) - \mathbf{Q}_i \cdot \mathbf{Q}_j \right] \\ & + g_{ij}^{\mathrm{IF}} \left[3(\mathbf{Q}_i \cdot \hat{\mathbf{n}}_{ij})(\hat{\mathbf{n}}_{ij} \cdot \mathbf{Q}_j) - \mathbf{Q}_i \cdot \mathbf{Q}_j \right] \\ & - g_{ij}^{\mathrm{FF}} \left[(\mathbf{Q}_i \cdot \hat{\mathbf{n}}_{ij})(\hat{\mathbf{n}}_{ij} \cdot \mathbf{Q}_j) - \mathbf{Q}_i \cdot \mathbf{Q}_j \right] \}, \end{aligned} \tag{2}$$

In this Hamiltonian we introduce the near, intermediate, and far-field coupling terms:

$g_{ij}^{\mathrm{NF}} = \frac{\alpha'_{sp}}{r_{ij}^3}\cos(kr_{ij})$, $g_{ij}^{\mathrm{IF}} = \frac{\alpha'_{sp}k}{r_{ij}^2}\sin(kr_{ij})$, and $g_{ij}^{\mathrm{FF}} = \frac{\alpha'_{sp}k^2}{r_{ij}}\cos(kr_{ij})$, respectively, with wavenumber $k = \sqrt{\varepsilon_b}\frac{\omega}{c}$. Additionally, r_{ij} is the distance between the ith and jth LSPRs and $\hat{\mathbf{n}}_{ij}$ is the unit vector connecting two LSPRs. We further incorporate retardation effects by considering the lattice dispersion in the polarizability,

$$\alpha'_{sp} = \frac{1}{\alpha_{sp}^{-1} - i\frac{2}{3}k^3}, \tag{3}$$

with $\alpha_{sp} = r_0^3\frac{3}{\varepsilon_\infty - 2\varepsilon_b}$. Including these terms, we have incorporated all retardation effects associated with point dipoles.[33]

It should be noted that this Hamiltonian, when diagonilzed, results in a transcendental equation. The eigenvalues of the Hamiltonian are functions of ω, which are the frequencies of the collective modes, that is, the eigenvalues are functions of themselves. In order to fully solve this problem, we make a first guess of ω for a particular mode of interest and iteratively compute the eigenvalues. Using the eigenvalue associated with the mode of interest, the Hamiltonian is diagonalized to convergence. The process is repeated for each mode of interest.

Results and Discussion

In this work, the monomer magnetic unit is a six-member ring, with silver nanoparticles located at the vertices of a regular hexagon. To model the individual nanoparticles, we employ a Drude model for silver where $\omega_p = 9.1$ eV, $\varepsilon_\infty = 3.77$, and $\gamma = 0.003$ eV. Note that we have greatly reduced the damping constant in order to better see the magnetic modes in the simulations. We explore and manipulate three magnetic oligomer systems: a twomer, a linear threemer, and a triangular threemer. The number of rings in a magnetic system corresponds to the number of magnetic modes in the system.[9] The twomer supports an in-phase mode (North-North, or NN) and an out-of-phase mode (North-South, or NS). The linear threemer supports an all in-phase mode (North-North-North, or NNN), a minimally

out-of-phase mode (North-Zero-South, or NZS), and a maximally out-of-phase mode (North-South-North, or NSN). The triangular threemer supports an all in-phase mode (North-North-North, or NNN) and two degenerate out-of-phase modes (North-South, or NS). These modes and their relative magnetic fields are depicted in Figures 1, 3, and 4. In each manipulation, the particles have radius r_0 and nearest-neighbor spacing r_{nn}. In the first set of model calculations, we compare to full-wave simulations to verify that the model accurately captures the properties of the systems, but beyond that we cease comparison to simulation in order to focus on the predictive power of the model. The first calculations, depicted in Figure 1 show how the magnetic modes of the twomer and threemers are impacted by the overall scale of the system. In these manipulations, the nearest neighbor distances are held at $r_{\text{nn}} = 3 \times r_0$ while r_0 varies from 1 nm to 30 nm.

In Figure 1a, the magnetic mode eigenvalues are computed for each system. The solid lines depict model calculations, and the dashed lines depict simulated results. Interestingly, the magnetic modes exhibit a dynamic energy ordering, switching order twice as a function of scale. It is presumable that they continue to flip at larger and larger sizes. This is confirmed by simulations, with the model overestimating the eigenvalues by about 0.6% and underestimating the crossing points by under a nanometer. These small errors are consistent across all three systems. Figure 1b displays the computed interaction strength for each eigenmode produced by the tight-binding model. In other words, we have plotted $\sum_{i>j} \mathbf{p}_i \cdot \mathbf{E}$ where $\mathbf{p}_i$ is an eigenvector and $\mathbf{E}$ is the field produced by the other dipoles. The interaction strength for each mode follows the same pattern as the eigenvalues, as expected, signifying that though this result is unexpected, it is not unphysical.

To more fully explore why the ordering of the eigenvalues would change with increasing size of the magnetic oligomers, we investigate the various parts of the fully retarded electric field. In Figure 2 we plot the near-, intermediate-, and far-field interaction strength, as well as the sum of those three terms, for the four possible arrangements of dipoles in a MNP dimer. The plots depict how the strength of the interaction varies with MNP separation

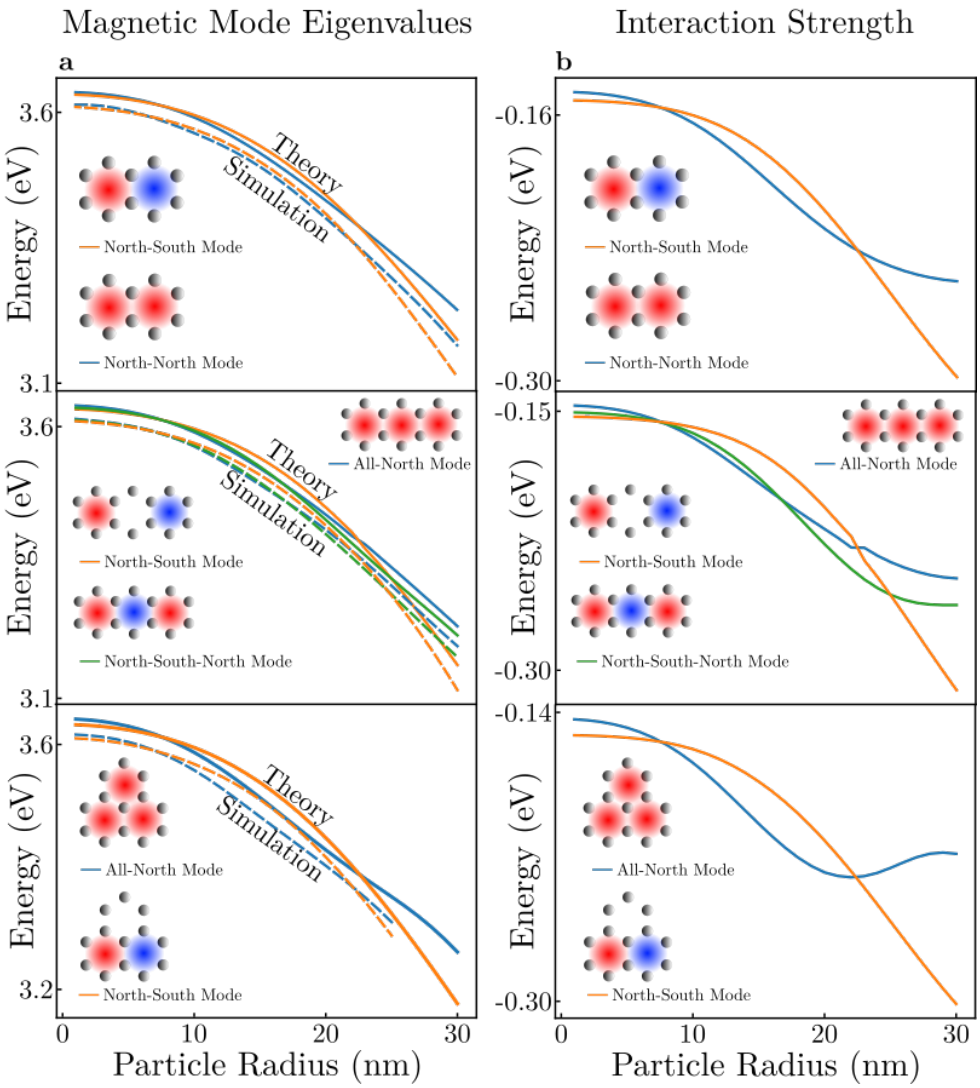

Figure 1: Magnetic mode eigenvalues (column a), predicted and simulated, and interaction strengths (column b) for the magnetic twomer (first row), linear threemer (second row), and triangular threemer (thir d row). All of the magnetic modes range from 3.6 eV to 3.1 eV. In each system, the magnetic modes exhibit multiple crossings, showing that the eigenspectrum of these magnetic systems depends on th eir scale. The model consistently overestimates the eigenvalues by 0.5 eV, and consistently underes timates the crossing points by less than a nanometer. The twomer has two magnetic modes, one in-pha se mode (blue trace) and one out-of-phase mode (orange trace). The linear threemer has three modes, an in-phase mode (blue trace), a minimally out-of-phase mode (orange trace), and a maximally out-of -phase mode (green trace). The triangular threemer exhibits three magnetic modes, but the out-of-phase mo des (orange trace) are degenerate so only one is depicted. The other mode is a maximally in-phase m ode (blue trace). To further emphasize the impact of scale, we have plotted the total interaction s trength of each eigenmode, *i.e.* the sum of each eigenvector's dot product with the electri c field of all of the other dipoles. This calculation reaffirms the scale dependence and predicts m ode crossings at the same scale as both the eigenvalue calculation and the simulations.

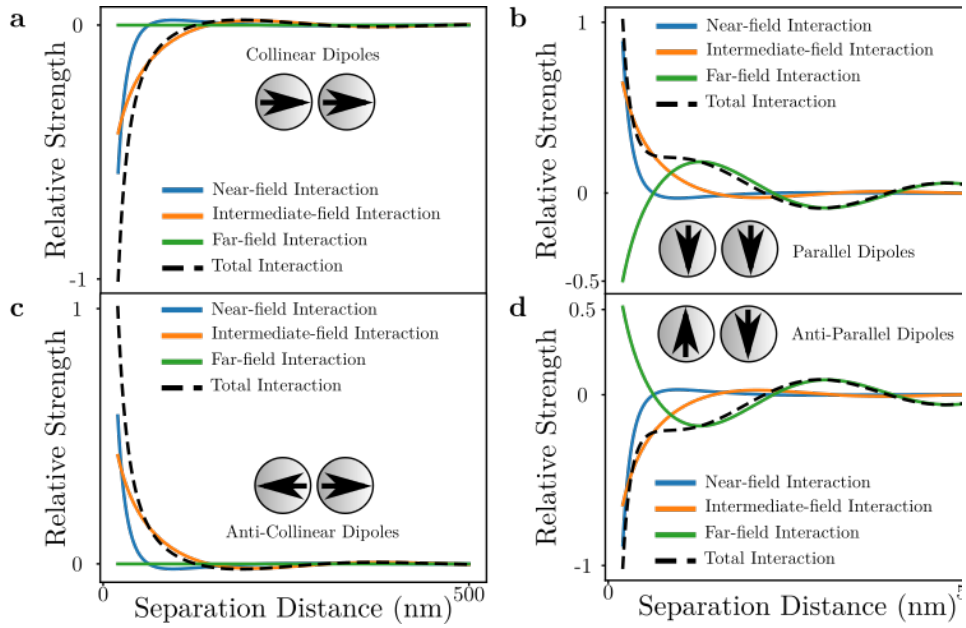

Figure 2: Relative interaction strengths for the four possible dipole arrangements of a nanoparticle dimer: collinear (a), parallel (b), anti-collinear (c), and anti-parallel (d). Plotted are the near-field (blue), intermediate-field (orange), far-field (green), and total (black, dashed) interaction strengths for each set of dipoles as a function of dipole-dipole distance. Interes tingly, and stemming from the form of the dipole relay tensor, the far-field interaction term is zero for both pairs of linear dipoles. From these plots, it can be seen that the favorability of a specific dipole arrangement depends on the separation between the dipoles. This can be seen in the fact that each part of the field depends differently on the separation, and each field term contains an oscillating term. At short length scales, the interaction is dominated by the near-field. However, as the distance increases, the interaction is dominated by the intermediate -field (a and c) or the far-field (b and d). As a result, there are separation distances at which normally unfavorable arrangements become favorable. Since magnetic oligomers can be describe through pairwise interactions of electric dipoles, it follows that the eigenvalues must also change order as different arrangements of electric dipoles become more and less favorable.

distance, and how much it depends on each of the field terms. There are two overall trends to point out. The first is that at small distances, the overall interaction is dominated by the near-field term due to its $\frac{1}{r_{ij}^3}$ dependence; at larger distances, the overall interaction follows the intermediate-field (Figure 2a and c) or the far-field (FIgure 2b and d). The second trend is the changing sign of the three field terms and the total interaction. This distance-dependent oscillatory nature directly contributes to the energy ordering of the eigenmodes, because its result is that different dipole arrangements are more favorable at different distances. In fact, it has been well documented that system length-scale has an oscillatory impact on its eigenenergies[26,34] So, it seems apparent that at some length scales, the dipole-dipole interactions in the North-South mode of the twomer are more favorable than those in the North-North mode, but that this favorability changes as a function of system size.

We have convinced ourselves that 1) the quasistatic, nearest-neighbors tight-binding model does not contain enough information to agree with fully retarded electrodynamics simulations, 2) those same simulations conform to the results from an updated tight-binding model that incorporates retardation effects and all-particle interactions and 3) the unexpected mode switching exhibited by these magnetic systems is entirely physical and explicable by the decaying and oscillatory distance-dependence of the electric field terms. With a working model and a basic physical understanding of these three systems, we can now conduct a series of experiments to look at its tunable properties. In the previous section, the scale of the systems was changed. However, this would be impossible to change in real-time in a laboratory. Now, we look at variables that can be manipulated in real time, namely, the dielectric constant of the embedding medium and the spacing between nanoparticles.

In order to justify the next set of model calculations, we refer to research on flowing liquid crystal over MNP aggregates and, in real-time, adjusting the refractive index of the MNP environment, influencing the resonance frequencies of the system.[35] We apply this concept to our tight-binding model to determine if this has any implications on the properties of magnetic oligomers. What we find is that, as expected, increasing the opacity of the

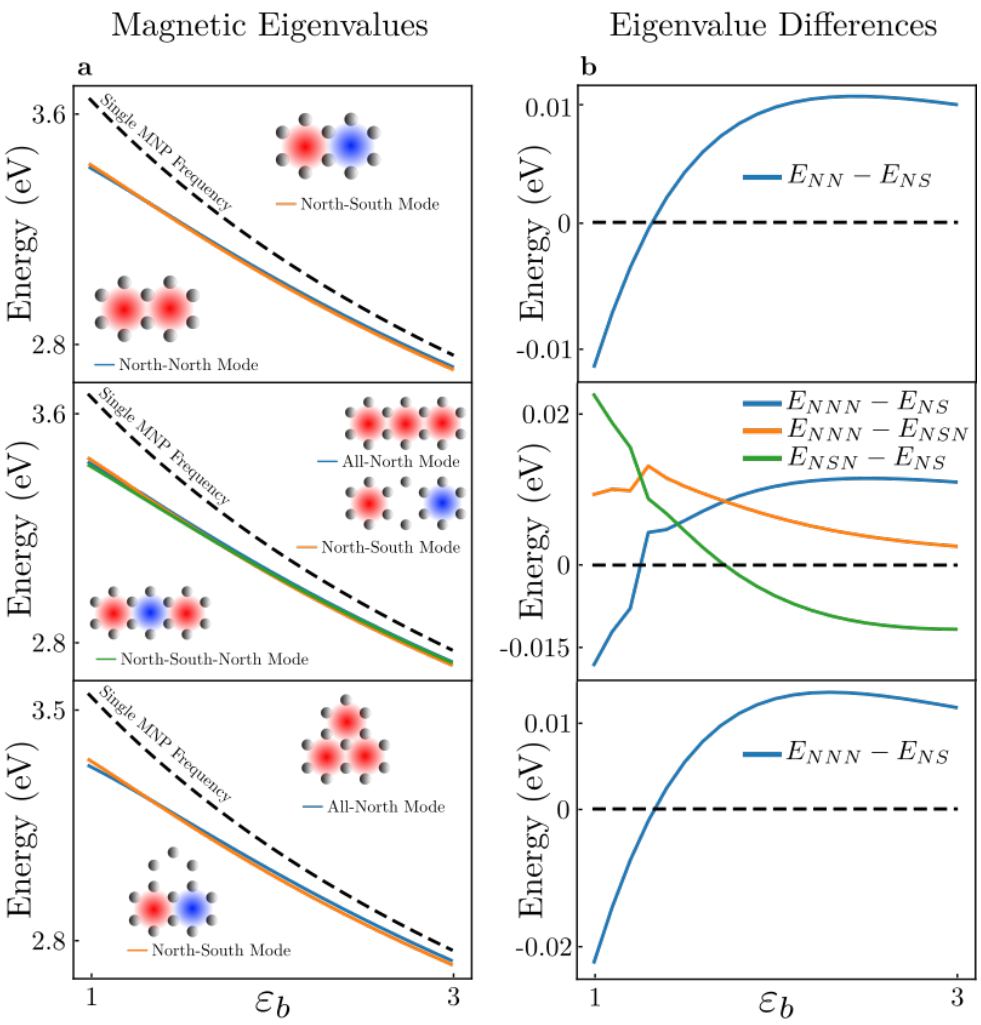

Figure 3: Magnetic mode eigenvalues (column a) for the twomer (first row), linear threemer (second row), and triangular threemer (third row) with particle sizes of 20 nm and magnetic mode eigenvalue differences (column b) as a function of the dielectric constant of an embedding medium. As the dielectric constant is increased from 1 to 3, the magnetic mode splitting approaches zero and the overall energy decreases. At very high dielectric values, the magnetic mode eigenvalues converge to the single particle resonance frequency. This can be explained by the increasing opacity of the medium effectively screening inter-particle interactions. It is also important to note that between $\varepsilon_b = 1$ and $\varepsilon_b = 1.5$, the magnetic modes differences vary sharply, either becoming much more positive or much more negative. This is indicative of mode-switching that is difficult to see in the eigenvalue plots. The increasing dielectric constant appears to have the same effect as increasing the scale of the system, as it recovers the same energy ordering for $r_0 > 20$ nm.

embedding medium decreases the resonance frequency of the collective modes. What we did not expect is that the embedding medium also influences the energy ordering of the eigenvalues. Results of one of our explorations are summarized in Figure 3. As the opacity of the medium increases, the eigenmodes collapse onto each other, and eventually converge with the single-particle frequency. Because the modes collapse so quickly and appear to overlap at all values of ε_b, Figure 3b displays the difference in energy between all of the eigenmodes of each system. The values of ε_b where the differences cross zero signfy mode-crossing. From these two observations we conclude that the opacity of the embedding medium weakens the overall inter-particle interactions. However, this occurs differently for each of the parts of the interaction. The near-field term contains no k-dependence, and so is reduced by one factor of ε_b. The intermediate-field term is linear in k, so it is reduced by a factor of $\sqrt{\varepsilon_b}$. Lastly, the far-field term is quadratic in k, so all ε_b-dependence is removed. At higher values of the dielectric constant the far-field term dominates, much like the way particles that are far apart interact primarily through their far-fields (Figure 2b and d). In other words, embedding magnetic systems in some dielectric medium causes them to act as though they are larger, effectively increasing their scale. This conclusion gives experimentalists an interesting way to tune these systems. Not only does it allow control over where in the spectrum the resonances occur, but it also gives a sense of control over which magnetic modes are accessible at which frequencies.

Other researchers have been working on the ability to reversibly tune the size of a plasmonic aggregate using various polymers[36] or DNA,[37,38] taking a collection of particles with fixed sizes and moving them back and forth to have different inter-particle spacings or a different arrangement. Here, we implement the idea of continuously distorting the nearest-neighbor spacing, from touching to tens of radii apart. We present data for particle radii of 15 nm and 30 nm in Figure 4a and b, respectively. The results of these model calculations are reminiscent of the results in Figure 2 in that the eigenmodes oscillate about each other as the particles move farther apart. In addition, similarly to Figure 3, at very large distances the

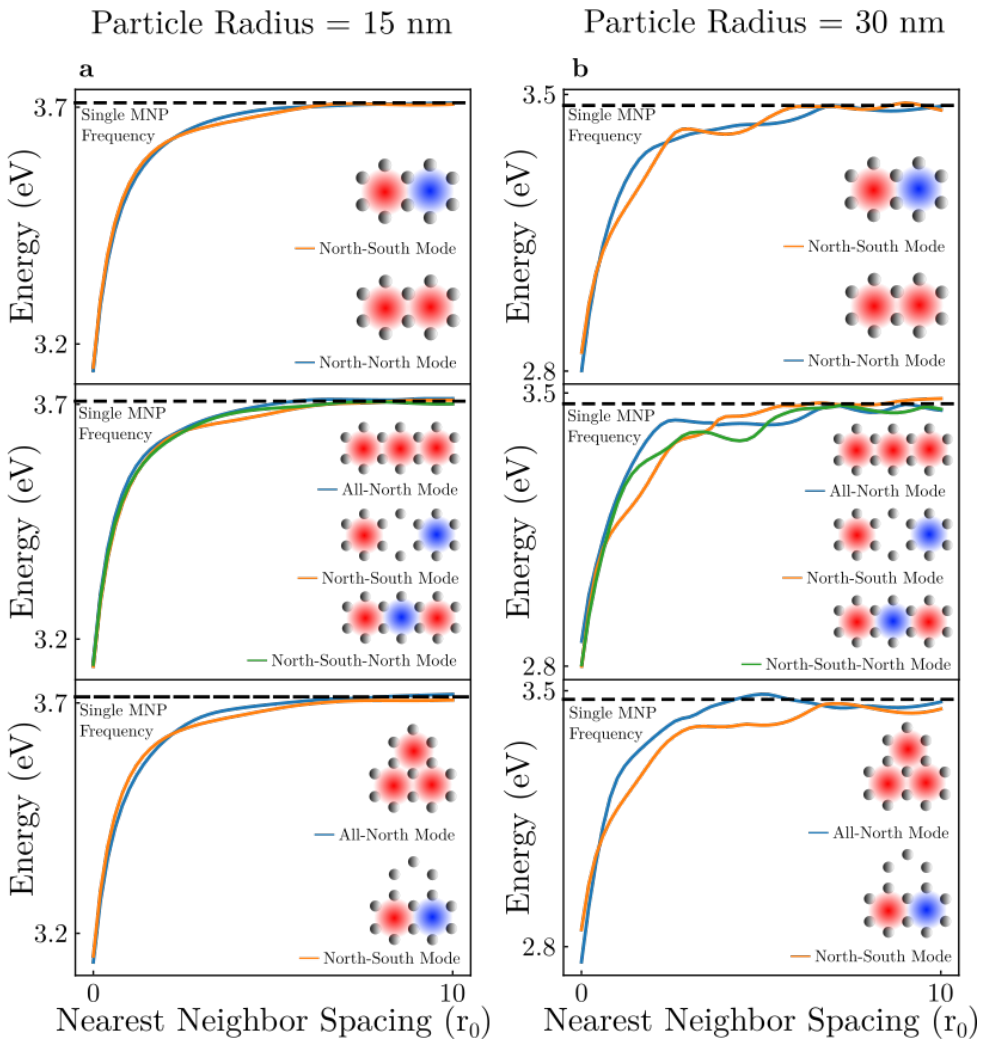

Figure 4: Magnetic mode eigenvalues for the twomer (first row), linear threemer (second row), and triangular threemer (third row) with particle sizes of 15 nm (column a) and 30 nm (column b) as a function of nearest neighbor particle spearation. The separation is plotted as a function of the particle size, in units of radii. It is important to note that as the separation distance increases, the magnetic modes cross multiple times and their eigenvalues converge to, and oscillate about the single particle frequency. This is a result of the decreasing interaction strength. In the limit of particles infinitely far away from each other, their interaction stength is zero. The oscillating nature of the eigenvalues is a result of the complex exponential dependence of the fields.

eigenvalues converge to the single LSPR frequency, exhibiting small amplitude oscillations. This is indicative of the coupling falling very near to zero. It is clear that this method, as opposed to the method of tuning the dielectric constant of the background, offers a much greater degree of tunability. Designing a system in which the inter-particle spacing could be varied in discrete steps would lead to the ability to directly choose the resonance frequency of a specific magnetic mode. Furthermore, being able to directly detect the frequency of the magnetic mode optically would even turn such magnetic systems into thermometers, pH probes, or detectors of any environmental factor that would change the size of the embedding polymer.

Conclusion

We have shown that magnetic oligomer systems composed of few monomer units exhibit tunable magnetic resonances to the extent that the researcher may influence the size, shape, and environment of the oligomers to choose the ordering of the normal modes. However, we stress that the systems studied in this work were chosen due to their theoretical simplicity. In simulated and experimental spectroscopies, these eigenmodes would overlap and be nearly indistinguishable. It has been shown that oligomers whose constituents are rod-like or elongated geometries have sharper, more isolated magnetic resonances.[10] To this end, future studies will involve these geometries to determine if they have the same eigenmode-switching properties and tunability. With this groundwork on the properties of small oligomers, there is now an incentive and an avenue to expanding the concepts presented here to larger aggregates, as well as a need to confirm the predictions made here with experiments. The ability of the researcher to decide the resonance frequency of a particular eigenmode opens the door to the ability to dynamically and actively determine system properties.

Acknowledgement

CEI, NSF, DOE?, Niket, some other people, probably, HPC.

References

1. Clippe, P.; Evrard, R.; Lucas, A. A. Aggregation Effect on the Infrared Absorption Spectrum of Small Ionic Crystals. *Phys. Rev. B* **1976**, *14*, 1715–1721.

2. Aravind, P.; Nitzan, A.; Metiu, H. The Interaction between Electromagnetic Resonances and its Role in Spectroscopic Studies of Molecules Adsorbed on Colloidal Particles or Metal Spheres. *Surf. Sci.* **1981**, *110*, 189 – 204.

3. Xu, Y. Electromagnetic Scattering by an Aggregate of Spheres. *Appl. Opt.* **1995**, *34*, 4573–4588.

4. Mishchenko, M. I.; Mackowski, D. W.; Travis, L. D. Scattering of Light by Bispheres with Touching and Separated Components. *Appl. Opt.* **1995**, *34*, 4589–4599.

5. Alù, A.; Salandrino, A.; Engheta, N. Negative Effective Permeability and Left-Handed Materials at Optical Frequencies. *Opt. Express* **2006**, *14*, 1557–1567.

6. Alù, A.; Engheta, N. Dynamical Theory of Artificial Optical Magnetism Produced by Rings of Plasmonic Nanoparticles. *Phys. Rev. B* **2008**, *78*, 085112.

7. Hentschel, M.; Dregely, D.; Vogelgesang, R.; Giessen, H.; Liu, N. Plasmonic Oligomers: The Role of Individual Particles in Collective Behavior. *ACS Nano* **2011**, *5*, 2042–2050, PMID: 21344858.

8. Brandl, D. W.; Mirin, N. A.; Nordlander, P. Plasmon Modes of Nanosphere Trimers and Quadrumers. *J. Phys. Chem. B* **2006**, *110*, 12302–12310.

9. Cherqui, C.; Bigelow, N. W.; Vaschillo, A.; Goldwyn, H.; Masiello, D. J. Combined Tight-Binding and Numerical Electrodynamics Understanding of the STEM/EELS Magneto-Optical Responses of Aromatic Plasmon-Supporting Metal Oligomers. *ACS Photonics* **2014**, *1*, 1013–1024.

10. Cherqui, C.; Wu, Y.; Li, G.; Quillin, S. C.; Busche, J. A.; Thakkar, N.; West, C. A.; Montoni, N. P.; Rack, P. D.; Camden, J. P. . *et al.* STEM/EELS Imaging of Magnetic Hybridization in Symmetric and Symmetry-Broken Plasmon Oligomer Dimers and All-Magnetic Fano Interference. *Nano Lett.* **2016**, *16*, 6668–6676, PMID: 27673696.

11. Karaveli, S.; Zia, R. Strong Enhancement of Magnetic Dipole Emission in a Multilevel Electronic System. *Opt. Lett.* **2010**, *35*, 3318–3320.

12. Noginova, N.; Zhu, G.; Mavy, M.; Noginov, M. Magnetic Dipole Based Systems for Probing Optical Magnetism. *J. Appl. Phys.* **2008**, *103*, 07E901.

13. Wang, J.; Fan, C.; He, J.; Ding, P.; Liang, E.; Xue, Q. Double Fano Resonances Due to Interplay of Electric and Magnetic Plasmon Modes in Planar Plasmonic Structure with High Sensing Sensitivity. *Opt. Express* **2013**, *21*, 2236–2244.

14. Zhu, Z.; Bai, B.; You, O.; Li, Q.; Fan, S. Fano Resonance Boosted Cascaded Optical Field Enhancement in a Plasmonic Nanoparticle-in-Cavity Nanoantenna Array and its SERS Application. *Light: Science and Applications* **2015**, *4*, e296.

15. Lee, K.-L.; Huang, J.-B.; Chang, J.-W.; Wu, S.-H.; Wei, P.-K. Ultrasensitive Biosensors Using Enhanced Fano Resonances in Capped Gold Nanoslit Arrays. *Scientific Reports* **2015**, *5*, 8547.

16. Wu, C.; Khanikaev, A. B.; Adato, R.; Arju, N.; Yanik, A. A.; Altug, H.; Shvets, G. Fano-Resonant Asymmetric Metamaterials for Ultrasensitive Spectroscopy and Identification of Molecular Monolayers. *Nat. Mat.* **2012**, *11*, 69–75.

17. Cetin, A. E.; Altug, H. Fano Resonant Ring/Disk Plasmonic Nanocavities on Conducting Substrates for Advanced Biosensing. *ACS Nano* **2012**, *6*, 9989–9995.

18. Zhang, S.; Bao, K.; Halas, N. J.; Xu, H.; Nordlander, P. Substrate-Induced Fano Resonances of a Plasmonic Nanocube: a Route to Increased-Sensitivity Localized Surface Plasmon Resonance Sensors Revealed. *Nano Lett.* **2011**, *11*, 1657–1663.

19. Liu, H.; Genov, D. A.; Wu, D. M.; Liu, Y. M.; Steele, J. M.; Sun, C.; Zhu, S. N.; Zhang, X. Magnetic Plasmon Propagation Along a Chain of Connected Subwavelength Resonators at Infrared Frequencies. *Phys. Rev. Lett.* **2006**, *97*, 243902.

20. Liu, N.; Mukherjee, S.; Bao, K.; Brown, L. V.; Dorfmüller, J.; Nordlander, P.; Halas, N. J. Magnetic Plasmon Formation and Propagation in Artificial Aromatic Molecules. *Nano Lett.* **2011**, *12*, 364–369.

21. Liu, N.; Mukherjee, S.; Bao, K.; Li, Y.; Brown, L. V.; Nordlander, P.; Halas, N. J. Manipulating Magnetic Plasmon Propagation in Metallic Nanocluster Networks. *ACS Nano* **2012**, *6*, 5482–5488.

22. Greybush, N. J.; Liberal, I. n.; Malassis, L.; Kikkawa, J. M.; Engheta, N.; Murray, C. B.; Kagan, C. R. Plasmon Resonances in Self-Assembled Two-Dimensional Au Nanocrystal Metamolecules. *ACS Nano* **2017**, *11*, 2917–2927, PMID: 28190335.

23. Hohenester, U.; Trügler, A. MNPBEM - A Matlab Toolbox for the Simulation of Plasmonic Nanoparticles. *Comp. Phys. Comm.* **2012**, *183*, 370 – 381.

24. Myroshnychenko, V.; Rodriguez-Fernandez, J.; Pastoriza-Santos, I.; Funston, A. M.; Novo, C.; Mulvaney, P.; Liz-Marzan, L. M.; Garcia de Abajo, F. J. Modelling the optical response of gold nanoparticles. *Chem. Soc. Rev.* **2008**, *37*, 1792–1805.

25. Turner, M. D.; Hossain, M. M.; Gu, M. The Effects of Retardation on Plasmon Hybridization within Metallic Nanostructures. *New J. of Phys.* **2010**, *12*, 083062.

26. Dahmen, C.; Schmidt, B.; von Plessen, G. Radiation Damping in Metal Nanoparticle Pairs. *Nano Lett.* **2007**, *7*, 318–322, PMID: 17243751.

27. Rechberger, W.; Hohenau, A.; Leitner, A.; Krenn, J.; Lamprecht, B.; Aussenegg, F. Optical Properties of Two Interacting Gold Nanoparticles. *Opt. Commun.* **2003**, *220*, 137 – 141.

28. Kottmann, J. P.; Martin, O. J. F. Retardation-Induced plasmon Resonances in Coupled Nanoparticles. *Opt. Lett.* **2001**, 1096–1098.

29. Haynes, C. L.; McFarland, A. D.; Zhao, L.; Van Duyne, R. P.; Schatz, G. C.; Gunnarsson, L.; Prikulis, J.; Kasemo, B.; Käll, M. Nanoparticle Optics: The Importance of Radiative Dipole Coupling in Two-Dimensional Nanoparticle Arrays. *J. Phys. Chem. B* **2003**, *107*, 7337–7342.

30. Bouhelier, A.; Bachelot, R.; Im, J. S.; Wiederrecht, G. P.; Lerondel, G.; Kostcheev, S.; Royer, P. Electromagnetic Interactions in Plasmonic Nanoparticle Arrays. *J. Phys. Chem. B* **2005**, *109*, 3195–3198, PMID: 16851340.

31. Kinnan, M. K.; Chumanov, G. Plasmon Coupling in Two-Dimensional Arrays of Silver Nanoparticles: II. Effect of the Particle Size and Interparticle Distance. *J. Phys. Chem. C* **2010**, *114*, 7496–7501.

32. Jackson, J. D. *Classical Electrodynamics*, 3rd ed.; Wiley: New York, NY, 1999.

33. Purcell, E. M.; Pennypacker, C. R. Scattering and Absorption of Light by Nonspherical Dielectric Grains. *Astrophys. J.* **1973**, *186*, 705–714.

34. Near-, middle-, and far-field dipolar interactions in gold nanoparticle arrays. 2016; pp 97240B–97240B–8.

35. Yang, A.; Hoang, T. B.; Dridi, M.; Deeb, C.; Mikkelson, M. H.; Schatz, G. C.;

Odom, T. W. Real-time tunable lasing from plasmonic nanocavity arrays. *Nature Comm.* **2015**, *6*, 6939.

36. Qian, Z.; Guye, K. N.; Masiello, D. J.; Ginger, D. S. Dynamic Optical Switching of Polymer/Plasmonic Nanoparticle Hybrids with Sparse Loading. *The Journal of Physical Chemistry B* **2017**, *121*, 1092–1099, PMID: 28075134.

37. Cheng, W.; Campolongo, M. J.; Cha, J. J.; Tan, S. J.; Umbach, C. C.; Muller, D. A.; Luo, D. Free-standing nanoparticle superlattice sheets controlled by DNA. *Nature Materials* **2009**, *8*, 519–525.

38. Kuzyk, A.; Urban, M. J.; Idili, A.; Ricci, F.; Liu, N. Selective control of reconfigurable chiral plasmonic metamolecules. *Science Advances* **2017**, *3*.

Graphical TOC Entry

Some journals require a graphical entry for the Table of Contents. This should be laid out "print ready" so that the sizing of the text is correct.
Inside the `tocentry` environment, the font used is Helvetica 8 pt, as required by *Journal of the American Chemical Society*.
The surrounding frame is 9 cm by 3.5 cm, which is the maximum permitted for *Journal of the American Chemical Society* graphical table of content entries. The box will not resize if the content is too big: instead it will overflow the edge of the box.
This box and the associated title will always be printed on a separate page at the end of the document.